Applied Catalysis B: Environmental 336 (2023) 122921

Contents lists available at ScienceDirect

Applied Catalysis B: Environmental

journal homepage: www.elsevier.com/locate/apcatb

Heterostructured $CoFe_{1.5}Cr_{0.5}S_3O$/COFs/$BiVO_4$ photoanode boosts charge extraction for efficient photoelectrochemical water splitting

Lina Wang [a], Jinming Zhang [a], Yi Li [a], Yanbiao Shi [b,*], Jingwei Huang [c], Qiong Mei [d], Lei Wang [c], Fei Ding [a], Bo Bai [a], Qizhao Wang [a,c,**]

[a] School of Water and Environment, Key Laboratory of Subsurface Hydrology and Ecological Effects in Arid Region of Ministry of Education, Chang'an University, Xi'an 710054, China
[b] School of Environmental Science and Engineering, Shanghai Jiao Tong University, Shanghai 200240, China
[c] College of Chemistry and Chemical Engineering, Northwest Normal University, Lanzhou 730070, Gansu, China
[d] School of Land Engineering, Chang'an University, Xi'an 710054, China

ARTICLE INFO

Keywords:
Photoelectrochemical
Water splitting
$BiVO_4$ photoanode
COFs
Charge extraction

ABSTRACT

Photoelectrochemical (PEC) water splitting can convert the inexhaustible solar energy into green and storable H_2 to tackle fossil crisis and meet carbon neutrality. $BiVO_4$ is regarded as a promising photoanode owing to its superior visible light absorption, moderate redox potentials and well chemical stability, but suffering from the rapid recombination of charge carriers and sluggish interfacial water oxidation kinetics. Herein, a heterostructured $CoFe_{1.5}Cr_{0.5}S_3O$/COFs/$BiVO_4$ photoanode was fabricated to accelerate charge carriers' separation and boost water oxidation. The spinel-type $CoFe_{1.5}Cr_{0.5}S_3O$ serving as the co-catalyst enabled to largely lower the overpotential of water oxidation, while COFs acting as an interlayer passivated the interfacial defect between $CoFe_{1.5}Cr_{0.5}S_3O$ and $BiVO_4$. Benefiting from the collaboration of $CoFe_{1.5}Cr_{0.5}S_3O$ co-catalyst and COFs interlayer, heterostructured $CoFe_{1.5}Cr_{0.5}S_3O$/COFs/$BiVO_4$ photoanode featuring with a prominent charge extraction efficiency reached an impressive water oxidation photocurrent of 5.1 mA cm^{-2} at 1.23 V vs. RHE under AM 1.5 G irradiation, higher than that of pristine $BiVO_4$, binary COFs/$BiVO_4$ and CFCOS/$BiVO_4$ photoanodes. This work demonstrated that heterostructured $BiVO_4$-based photoanode with co-catalyst and interlayer enables to simultaneously enhance charge carrier utilization efficiency and optimize surface catalysis kinetics for efficient solar-to-fuel conversion.

1. Introduction

Solar-driven PEC water splitting is a sustainable, easily scalable and eco-friendly pathway to convert and store abundant solar energy into chemical bonds of fuels [1,2]. Among the previously reported photoanodes, $BiVO_4$ is one of most promising candidates owing to its small band gap (2.4 eV), low onset potential for oxygen evolution and suitable conduction band (CB) potential for H^+/H_2 redox reaction [3,4]. However, the rapid recombination of photoinduced charge carriers and sluggish interfacial water oxidation kinetics of $BiVO_4$ severely restricted its PEC water splitting performance.

Surface modification with suitable co-catalysts has demonstrated to be a deliverer to improve the PEC water splitting performance of photoanodes, especially for $BiVO_4$. This is because the decorated co-catalysts enable to simultaneously suppress charge carriers' recombination, provide sufficient reactive sites and minimize the overpotential of oxygen evolution reaction (OER) [5,6]. Among these developed co-catalysts (metallic oxides, hydroxides, phosphides and sulfides) [7–9], our previous works demonstrated that the spinel-type binary metallic oxides ($NiFe_2O_4$ [10], $CoFe_2O_4$ [10] and $ZnCo_2O_4$ [11,12]) exhibited superior activity to boost PEC water splitting efficiency of porous $BiVO_4$. More recently, Bi et al. demonstrated that $NiCo_2O_4$/Mo:$BiVO_4$ photoanode featuring with dual-metal active sites could accelerate bulk photo-hole extraction and reduce thermodynamics barrier of H_2O activation by the abundant surface oxygen vacancy, finally reaching a remarkable PEC efficiency [13]. However, the coupling of

* Corresponding author.
** Corresponding author at: School of Water and Environment, Key Laboratory of Subsurface Hydrology and Ecological Effects in Arid Region of Ministry of Education, Chang'an University, Xi'an 710054, China
E-mail addresses: shiyanbiao@sjtu.edu.cn (Y. Shi), wangqizhao@163.com, qzwang@chd.edu.cn (Q. Wang).

https://doi.org/10.1016/j.apcatb.2023.122921
Received 4 May 2023; Received in revised form 22 May 2023; Accepted 25 May 2023
Available online 26 May 2023

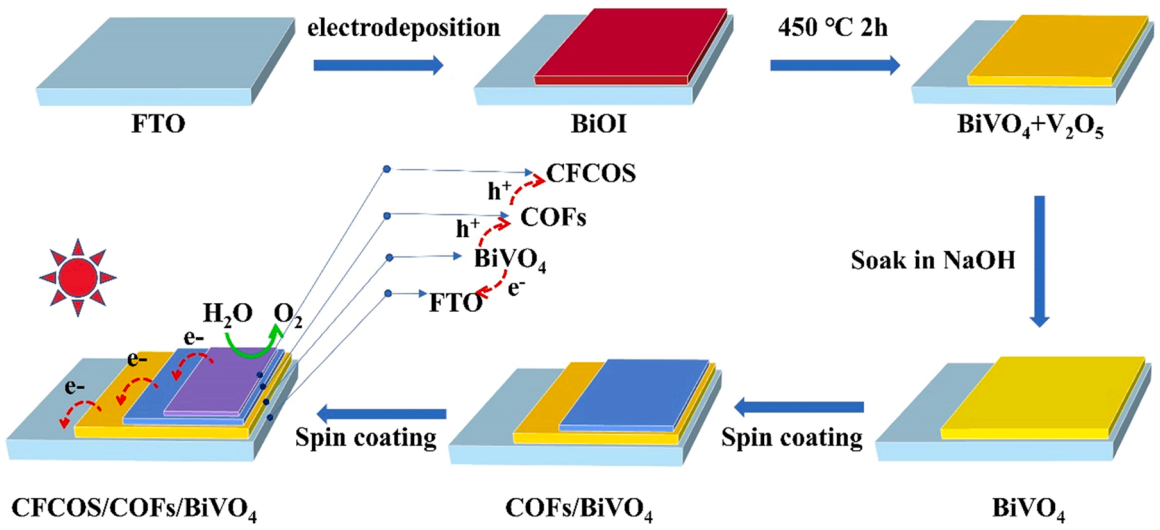

Scheme 1. Schematic illustration of the preparation of CFCOS/COFs/$BiVO_4$ photoanode.

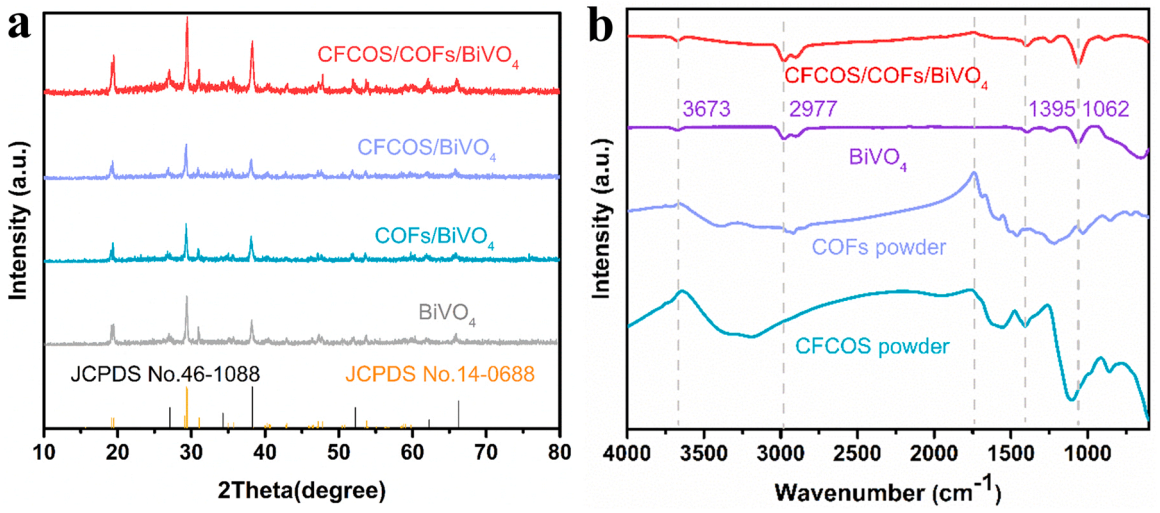

Fig. 1. (a) XRD patterns of $BiVO_4$, COFs/$BiVO_4$, CFCOS/$BiVO_4$ and CFCOS/COFs/$BiVO_4$. (b) FTIR spectra of pristine COFs, CFCOS, $BiVO_4$ and CFCOS/COFs/$BiVO_4$ photoanode.

co-catalysts and photoanodes easily resulted in the formation of interfacial defect, a universal charge carriers′ recombination center, further retarding water oxidation kinetics.

Recently, Li et al. reported that implanting a passivation layer between the Si-based photoanode and cocatalysts enabled to diminish the inherent interfacial defects and reach a record fill factor [14]. Likewise, the impending goals for $BiVO_4$ photoanode with spinel-type co-catalysts modification are to eliminate the inherent interfacial defects, facilitate the separation of electron-hole pairs and reduce the interfacial charge transport resistance. To address all these matters, a molecularly designed conjugated structure with efficient charge transfer channel is highly desirable [15–18]. Covalent organic frameworks (COFs) are typically porous crystalline polymers, which is formed by the assembly of single or multiple organic ligands linked through covalent bonds. As a rising-star 2D or 3D porous organic polymers, COFs has periodic backbones and ordered structures and channels. In the photoelectrochemical fields, COFs are usually deemed as the promising candidates because the inherent π-π interaction between adjacent layers and strong lateral π orbitals conjugation donates it with high-rate charge carrier mobility [19–21]. Therefore, embedding a COFs-based interlayer layer between $BiVO_4$ photoanode and spinel-type co-catalyst seems to be a feasible strategy to simultaneously boost the interfacial charge carrier kinetic and minimize the thermodynamics barrier of water oxidation.

In this work, we loaded the spinel-type $CoFe_{1.5}Cr_{0.5}S_3O$ (CFCOS) and COFs onto $BiVO_4$ surface to fabricate heterostructured CFCOS/COFs/$BiVO_4$ photoanode via a successive spin-coating process. The modified CFCOS aims to optimize the thermodynamic water oxidation of $BiVO_4$, while the embedded π-conjugated COFs between CFCOS and $BiVO_4$ film is expected to function as an interlayer layer to eliminate the inherent interfacial defects and accelerate charge carriers′ separation. After further optimizing the loading amount of co-catalyst and thickness of interlayer layer, heterostructured CFCOS/COFs/$BiVO_4$ photoanode exhibited a prominent photocurrent density of 5.1 mA cm^{-2} at 1.23 V vs. RHE under AM 1.5 G irradiation, reaching an impressive H_2 and O_2 production of 234.30 μmol cm^{-2} and 117.15 μmol cm^{-2} within 3 h, respectively, which is about 19 times enhancement of pristine $BiVO_4$.

2. Experimental section

2.1. Synthesis of COFs

COFs powder was synthesized via a solvent thermal condensation

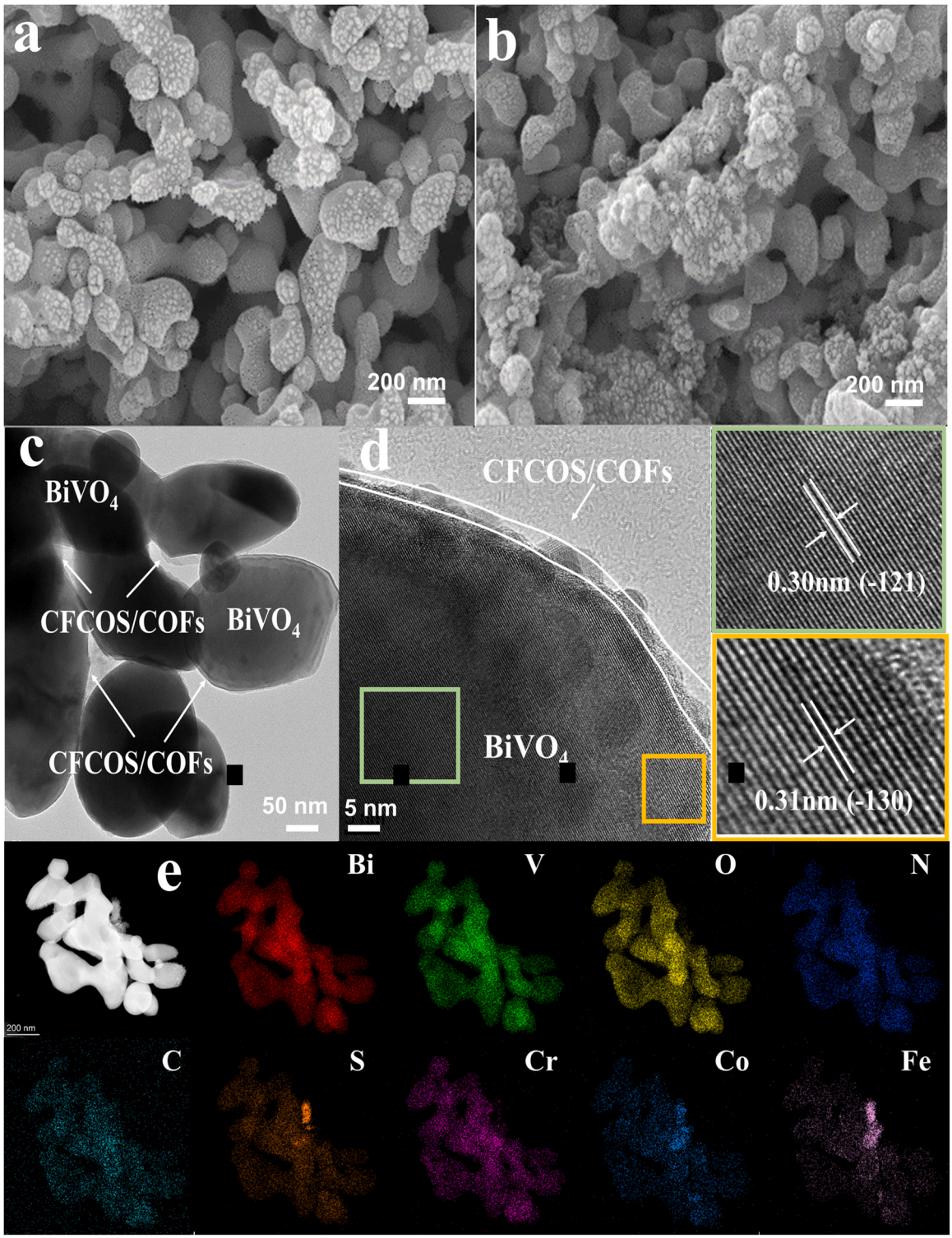

Fig. 2. SEM images of (a) pristine $BiVO_4$ and (b) heterostructured CFCOS/COFs/$BiVO_4$ films. (c) TEM, (d) HRTEM images and (e) TEM-EDS mapping of CFCOS/COFs/$BiVO_4$ film.

reaction. Typically, hexanone cyclohexane octahydrate (18.7 mg) and 1, 2, 4, 5-tetraaminobenzoquinone (15.2 mg) were dissolved into the mixture (2 mL) of ethylene glycol and acetic acid (3.0 M), where the volumes ratio of ethylene glycol and 3.0 M acetic acid is 1:1 (Scheme S1). The above solution was then transferred into a 20 mL Pyrex tube under nitrogen atmosphere and sonicated for 20 min. Finally, the Pyrex tube was heated at 65 ℃ for 4 h and subsequently raised to 120 ℃ for another 96 h. Finally, the obtained sample was washed and dried.

2.2. Synthesis of CFCOS powder

0.375 mmol of $Co(NO_3)_2$•6 H_2O, 0.75 mmol of $Fe(NO_3)_3$•9 H_2O, 0.19 mmol of sodium citrate, 3.3 mmol of urea and 2.5 mmol of polyacrylamide (PAM) were dissolved into 30 mL of deionized water and stirred under ambient temperature for 3 h. The suspension was then heated in stainless steel autoclave (200 °C, 12 h). After the autoclave naturally cooling down, $Cr(NO_3)_2$•6 H_2O (0.26 mmol) and Na_2S•9 H_2O

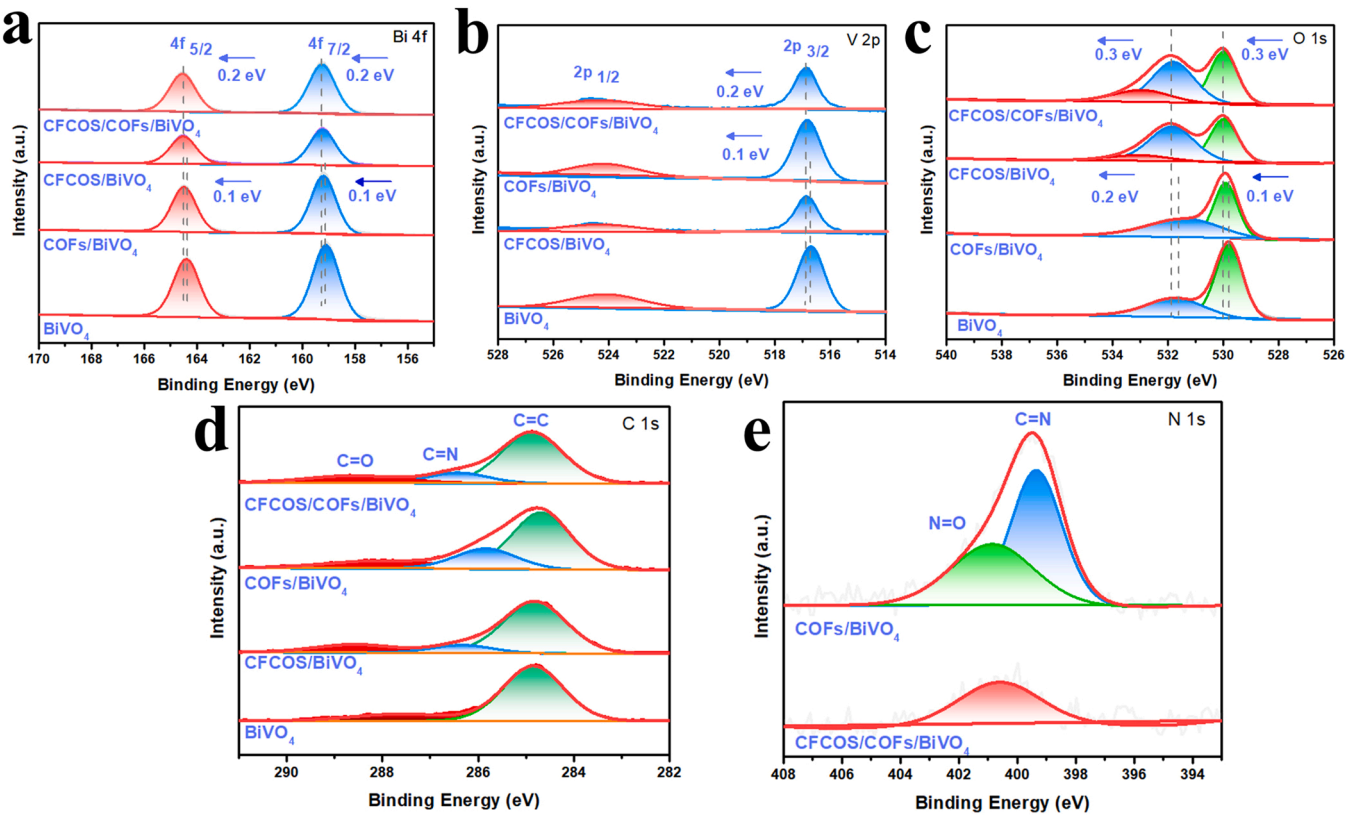

Fig. 3. High-resolution XPS spectra of CFCOS/COFs/$BiVO_4$, CFCOS/$BiVO_4$, COFs/$BiVO_4$ and $BiVO_4$ photoanodes, respectively: (a) Bi 4 f, (b) V 2p, (c) O 1 s, (d) C 1 s and (e) N 1 s.

(1.125 mmol) were directly added into the above suspension without further treatment. The mixture was further heated at 180 °C for another 12 h. Finally, the collected black powder was washed and dried in a vacuum oven at 60 °C. The as-prepared black powder was named as $CoFe_{1.5}Cr_{0.5}S_3O$ based on the results from XPS analysis (Table S1).

2.3. Preparation of COFs photoanode

COFs (10 mg) powder was dispersed into 1 mL of diluted Nafion solution (containing 30 μL of raw Nafion solution) and sonicated to form homogeneous solution. 80 μL of above solution was dropped onto FTO surface, which was then spinning-coating at 2500 rpm for 20 s. This step was repeated for several times to ensure the homogeneous coating of COFs onto FTO photoanode. The as-prepared sample was dried in an oven at 60 ℃ for 30 min to obtain COFs photoanode.

2.4. Preparation of CFCOS photoanode

CFCOS (10 mg) powder was dispersed into 1 mL of diluted Nafion solution (containing 30 μL of raw Nafion solution) and sonicated to form homogeneous solution. 80 μL of above solution was dropped onto FTO surface, which was then spinning-coating at 2500 rpm for 20 s. This step was repeated for 8 times to ensure the homogeneous coating of CFCOS onto FTO photoanode. The as-prepared sample was dried in an oven at 60 ℃ for 30 min to obtain CFCOS photoanode.

2.5. Preparation of heterostructured CFCOS/COFs/$BiVO_4$ photoanode

COFs (10 mg) and CFCOS (10 mg) powder was respectively dispersed into 1 mL of diluted Nafion solution (containing 30 μL of raw Nafion solution) and sonicated to form homogeneous solution A and B. Then, 80 μL of A solution was dropped onto $BiVO_4$ surface, which was spinning-coating at 2500 rpm for 20 s. This step was repeated for several times to ensure the homogeneous coating of COFs onto $BiVO_4$ photoanode. The as-prepared sample was dried in an oven at 60 ℃ for 30 min. Subsequently, 80 μL of B solution was dropped onto the COFs/$BiVO_4$ photoanode and the spin-coating operation repeated as the described above. For comparison, a series of CFCOS/COFsBiVO_4 photoanode were prepared with different spin coating numbers of 4, 6, 8, 10 and 12, respectively. Meanwhile, a binary CFCOS/$BiVO_4$ photoanode was prepared through the same process without the spin-coating of COFs.

2.6. Materials characterization

Microstructure of sample was characterized by scanning electron microscopy (SEM, GeminiSEM 300, ZEISS) and transmission electron microscopy (TEM, F200X G2, FEI Talos). Elemental distribution of sample was analyzed by energy dispersive spectroscopy (EDS). X-ray diffractometer (XRD) was recorded by Rigaku (D/max-IIIB, Japan) with Cu Kα as the radiation source. The molecular structure of samples was analyzed by Fourier transform infrared spectroscopy (FT-IR, Thermo Scientific Nicolet iS20). X-ray photoelectron spectrometer (XPS) analysis of all samples was performed with an energy spectrometer (Thermo Scientific K-Alpha). UV–visible diffuse reflectance spectra of samples (UV–vis DRS) was characterized by UV–vis spectrophotometer (U-3010). The charge separation efficiency was analyzed by Photoluminescence spectroscopy (PL, Hitachi F-4500).

2.7. PEC measurements

PEC performance of photoanodes was evaluated in a standard three-electrode system (CHI 760e, Shanghai Chenhua Instruments Co., Ltd., China), containing photoanodes as working electrode, Ag/AgCl electrode (3.5 M KCl) as reference electrode, and platinum as counter electrode. PEC performance tests were carried out in a rectangular quartz reactor (5 cm × 5 cm × 7 cm) with potassium borate aqueous

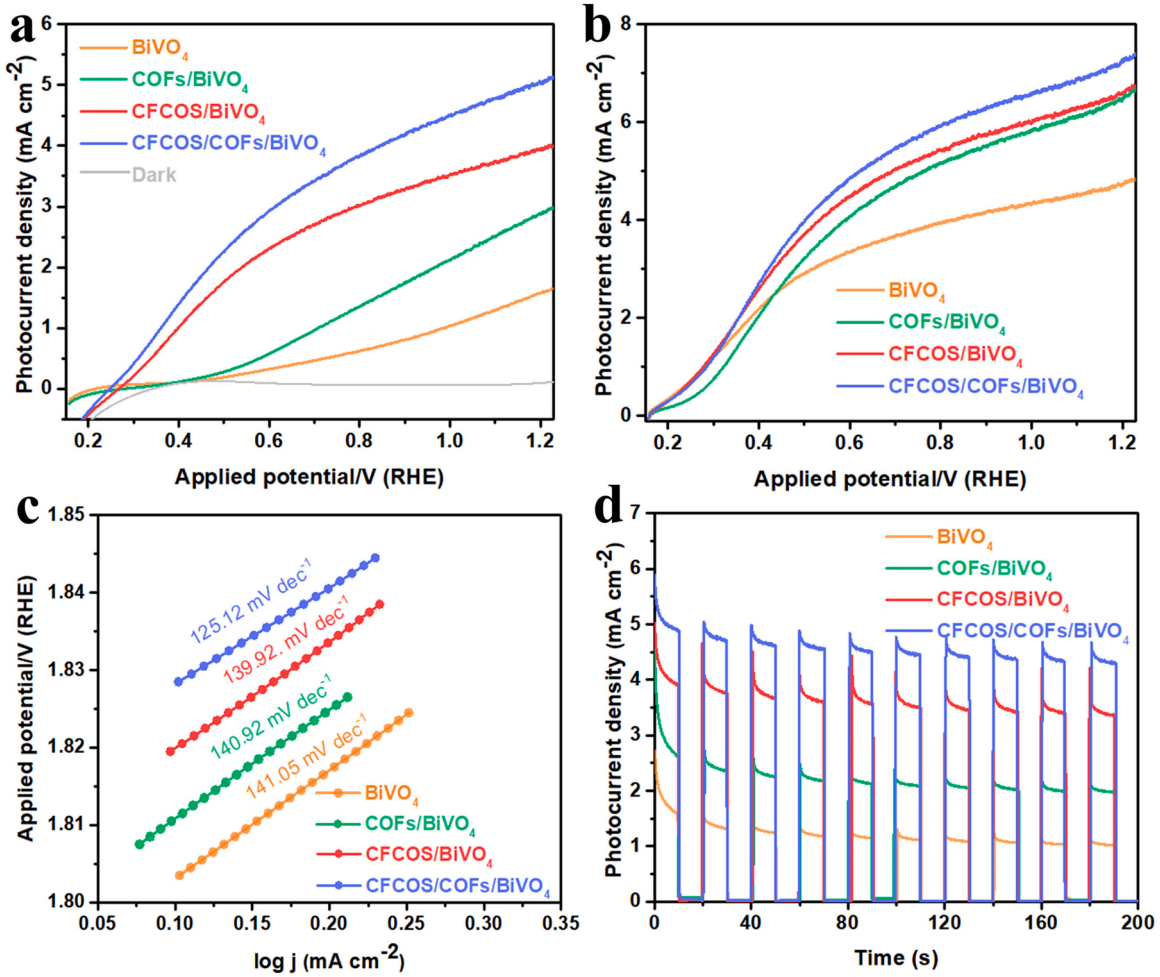

Fig. 4. (a) LSV curves with a scan rate of 50 mV s^{-1} in 1 M KBi solution (pH 9.5), (b) LSV curves in the presence of 1 M Na_2SO_3 with a scan rate of 50 mV s^{-1}, (c) Tafel slope and (d) I-t curves for CFCOS/COFs/$BiVO_4$, CFCOS/$BiVO_4$, COFs/$BiVO_4$ and $BiVO_4$ photoanodes.

solution (KBi, 1 M, pH 9.5) as the electrolyte. The effective active area of working electrode was about 1 cm^{-2}. A Xenon Lamp Source (Microsolar300, Beijing Perfectlight Technology Co., Ltd, China) with a transmittance $\lambda \geq 420$ nm filter was employed to evaluate the PEC performance of samples. The light intensity was corrected to 100 mW cm^{-2} with an optical power meter. Linear sweep voltammetry (LSV) was performed with a scan rate of 50 mV s^{-1} in the potential interval of −0.6–1.0 V vs. Ag/AgCl. Electrochemical impedance spectroscopy (EIS) was carried out in the frequency range of 0.1 Hz to 100 kHz with 1.2 V vs. RHE as the initial voltage. The generated H_2 and O_2 from PEC water splitting were monitored by gas chromatography (GC-9560, Shanghai Huaai Chromatography Technology Co., Ltd.).

3. Results and discussion

3.1. Material characterizations

Heterostructured CFCOS/COFs/$BiVO_4$ photoanode was prepared via a successive spin-coating process (Scheme 1). Briefly, $BiVO_4$ film was electrochemically deposited onto the FTO substrate. Subsequently, the precursors of COFs and CFCOS were orderly loaded on $BiVO_4$ surface.

The crystal structure of pristine $BiVO_4$, COFs/$BiVO_4$, CFCOS/$BiVO_4$ and heterostructured CFCOS/COFs/$BiVO_4$ photoanodes were identified by XRD patterns (Fig. 1a). Except for the characteristic peaks belonging to FTO substrate (JCPDS No. 46–1088), all diffraction peaks were attributed to monoclinic $BiVO_4$ (JCPDS No. 14–0688) [7,22]. No any peak belonged to CFCOS or COFs was found, which might be attributed to their low loading dosage and uniform dispersion on $BiVO_4$ surface (Fig. 1a). To verify the existence of CFCOS and COFs in the CFCOS/COFs/$BiVO_4$ film, FT-IR spectra of pristine $BiVO_4$, CFCOS, COFs and CFCOS/COFs/$BiVO_4$ were characterized (Fig. 1b). The peaks locating at 1062, 1243, 1395, 2977, 2091 and 3673 cm^{-1} were assigned to the characteristic FT-IR peaks of $BiVO_4$ [23,24]. As for the peak (1740 cm^{-1}) emerged in the CFCOS/COFs/$BiVO_4$ film, it well agreed with the characteristic peak of COFs. Besides, a much stronger FT-IR peak at 1062 cm^{-1} belonged to the CFCOS in CFCOS/COFs/$BiVO_4$. Based on the above results, we confirmed that CFCOS/COFs/$BiVO_4$ photoanode was successfully synthesized.

The micromorphology of as-prepared samples was characterized by SEM and TEM. It is obvious that the electrochemically deposited $BiVO_4$ film on FTO substrate was composed of irregular nanoparticles (Figs. 2a, S1a). Compared with the counterparts, the successive deposition of COFs and CFCOS of heterostructured CFCOS/COFs/$BiVO_4$ film did not obviously affect the basic morphology of $BiVO_4$ (Figs. 2b and S1b-d, S2). As displayed in the TEM and HRTEM images of CFCOS/COFs/$BiVO_4$, the clear lattice spacing of 0.26 nm and 0.31 nm corresponds to the (−121) and (−130) facets of $BiVO_4$ (Fig. 2c-d), respectively. A distinct interface between $BiVO_4$ film and CFCOS/COFs amorphous layer was observed, manifesting that $BiVO_4$ film was tightly packed by the CFCOS/COFs layer. The uniform distribution of Bi, V, O, N, C, S, Cr, Co and Fe in the heterostructured CFCOS/COFs/$BiVO_4$ film was further validated by the TEM-EDS mapping and elemental distribution profiles (Figs. 2e, S3).

Surface composition and elemental chemical states of as-prepared samples were analyzed by XPS spectra. Compared with pristine $BiVO_4$,

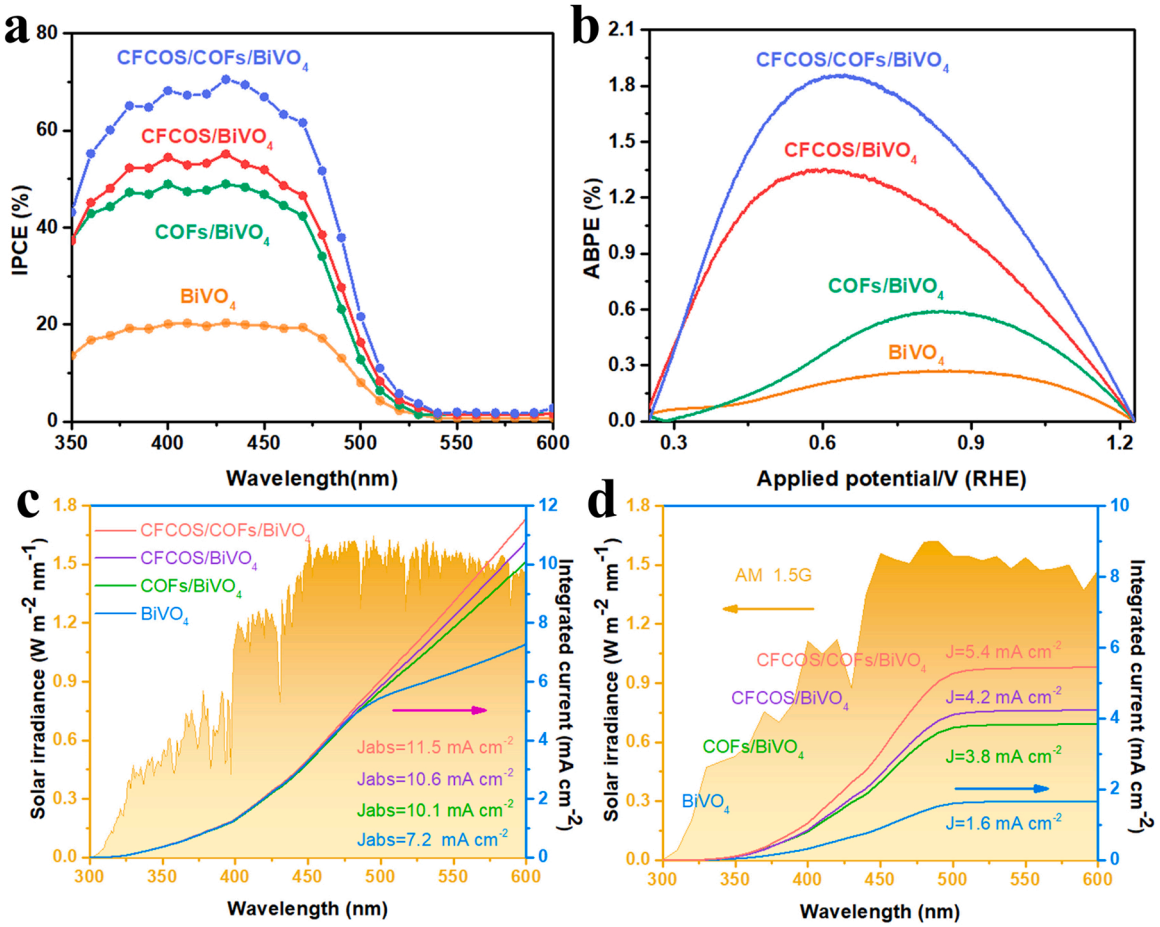

Fig. 5. (a) ABPE values, (b) IPCE values, solar irradiance of AM 1.5 G (ASTM G173–03) and (c) integrated photocurrent (J_{abs}), (d) calculated photocurrent densities of $BiVO_4$, (b) $COFs/BiVO_4$, $CFCOS/BiVO_4$ and (d) $CFCOS/COFs/BiVO_4$ photoanodes.

the peaks of Bi 4 f, V 2p and O 1 s spectra in $COFs/BiVO_4$, $CFCOS/BiVO_4$ and $CFCOS/COFs/BiVO_4$ consistently shifted to higher binding energies, suggesting that the introduction of CFCOS and COFs altered the coordination environment around $BiVO_4$ (Figs. 3a-c and S4a). High-resolution O ls XPS spectra were deconvoluted into three peaks locating at 529.9, 531.8 and 532.9 eV, which are assigned to the lattice oxygen, adsorbed oxygen and C═O group, respectively [6]. The successful coating of COFs onto $BiVO_4$ surface was demonstrated by the characteristic C═N groups of COFs emerged in high-resolution C 1 s (286.4 eV) and N 1 s (399.3 eV) XPS spectra (Fig. 3d-e) [25,26]. Moreover, the existence of S, Cr, Co and Fe in heterostructured CFCOS/COFs/$BiVO_4$ film was also demonstrated by XPS spectra (Fig. S4) [6]. Combined with the above results, we confirmed that heterostructured $CFCOS/COFs/BiVO_4$ photoanode was successfully constructed.

3.2. PEC measurements

The PEC water splitting performance of photoanodes was evaluated in 1 M KBi solution (pH 9.5). Under AM 1.5 G illumination (100 mW cm^{-2}), pristine $BiVO_4$ photoanode exhibited a relatively low photocurrent density of 1.6 mA cm^{-2} at 1.23 V vs. RHE due to the sluggish hole transfer kinetics between the interface of $BiVO_4$ and water molecule (Fig. 4a). To confirm this issue, a PEC sulfite oxidation reaction was carried out with Na_2SO_3 as the hole scavenger [5,27]. Noteworthily, the photocurrent density of $BiVO_4$ photoanode was promoted to 4.5 mA cm^{-2} (Fig. 4b), suggesting the necessity of loading OER co-catalysts onto $BiVO_4$ surface to facilitate the transfer of hole-to-electrolyte. As expected, the loading of CFCOS onto $BiVO_4$ photoanode enabled to increase the photocurrent density from 1.6 to 4.0 mA cm^{-2} at 1.23 V vs. RHE and decrease the onset potential from 0.40 to 0.26 V vs. RHE. The water oxidation reaction kinetics was further revealed by the electrochemical polarization tests and Tafel slope of $BiVO_4$, $COFs/BiVO_4$, $CFCOS/BiVO_4$ and $CFCOS/COFs/BiVO_4$ electrodes. Compared with pristine $BiVO_4$, the $CFCOS/BiVO_4$ electrode showed a significantly enhanced oxygen evolution activity (Fig. S5). Meanwhile, the smaller Tafel slope of $CFCOS/BiVO_4$ (139.92 mV dec^{-1}) indicated that the introduction of CFCOS indeed promoted the PEC water oxidation process of $BiVO_4$ (Fig. 4c). However, the measured photocurrent density of $CFCOS/BiVO_4$ in Na_2SO_3 solution was still far from its theoretical value. This is because the excess charge carriers' accumulating at the interface of $CFCOS/BiVO_4$ photoanode hindered the injection of charges into the electrolyte [28,29]. Therefore, a COFs interlayer featuring with high charge carrier mobility was subtly introduced to optimize the PEC performance of $CFCOS/BiVO_4$ photoanode. For the optimized heterostructured $CFCOS/COFs/BiVO_4$ photoanode, its photocurrent density reached at 5.1 mA cm^{-2} at 1.23 V vs. RHE (Fig. S6). Different from the $CFCOS/BiVO_4$ photoanode which displayed the particularly pronounced spike-like hill, heterostructured CFCOS/COFs/$BiVO_4$ photoanode significantly inhibited the sharp photocurrent attenuation (Fig. 4d), demonstrating the promotion of COFs interlayer on the interfacial charge transfer between $BiVO_4$ substrate and CFCOS co-catalyst.

The conversion efficiency of photon-to-charge was calculated based on the applied bias photon-to-current efficiency (ABPE) (Please see the detailed information in Text S2). Excitingly, heterostructured CFCOS/$COFs/BiVO_4$ photoanode exhibited the highest efficiency of 1.85% at the bias voltage of 0.62 V, surpassing $BiVO_4$, $COFs/BiVO_4$, $CFCOS/BiVO_4$ and the previously reported photoanodes (Fig. 5a, Table S2).

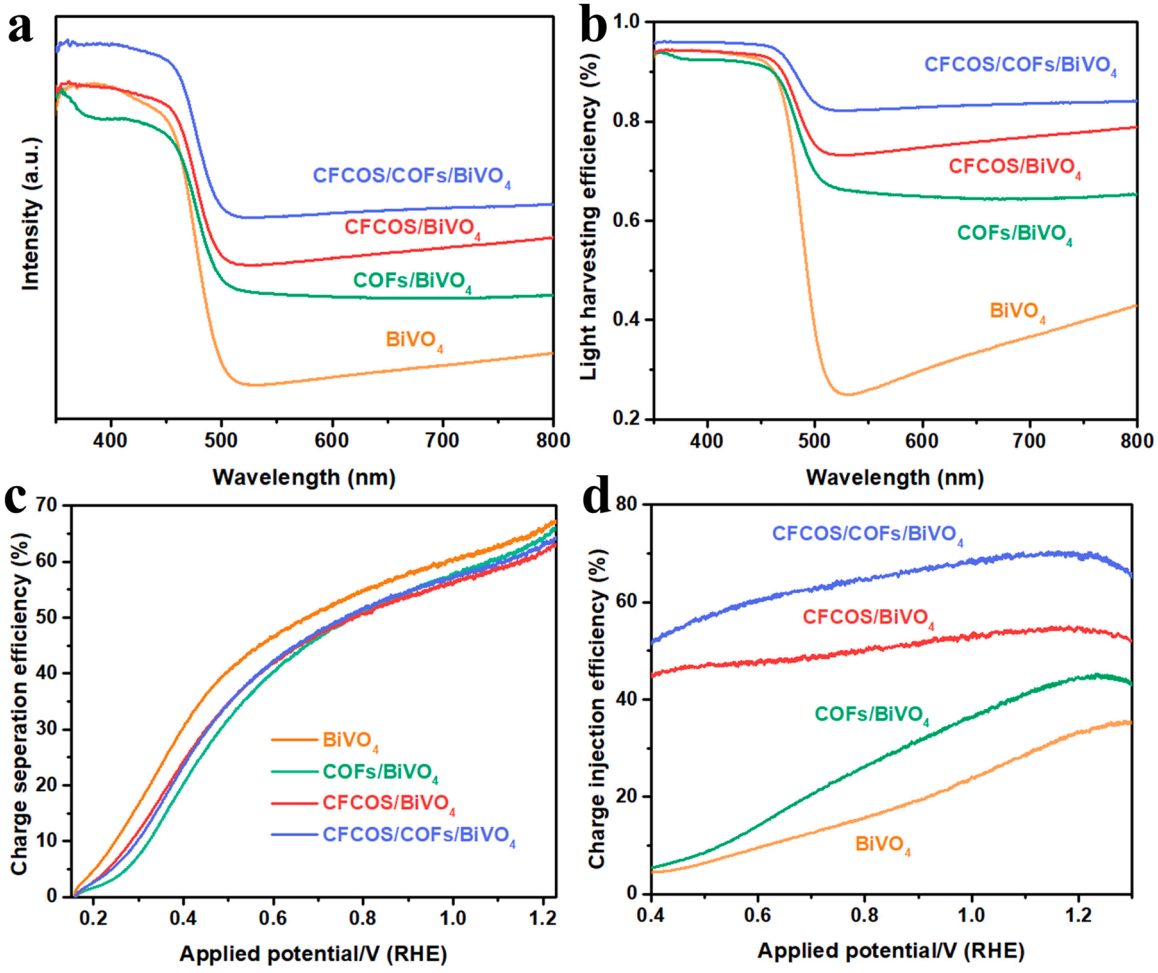

Fig. 6. (a) UV–vis diffuse reflectance spectra, (b) light absorption efficiency, (c) charge injection efficiencies and (d) charge separation efficiencies for $BiVO_4$, COFs/$BiVO_4$, CFCOS/$BiVO_4$ and CFCOS/COFs/$BiVO_4$ electrodes.

Benefiting from the increased photocurrent density at lower bias voltage, heterostructured CFCOS/COFs/$BiVO_4$ photoanode also showed the smallest voltage of the maximum ABPE than that of counterparts. The enhanced energy conversion efficiency of photoanodes could also be verified by the incident photon to current conversion efficiency (IPCE) value at a certain wavelength (Text S3). As displayed in Fig. 5b, the modification of $BiVO_4$ with CFCOS or COFs could effectively improve the IPCE value. While their assembly, that is heterostructured CFCOS/COFs/$BiVO_4$ photoanode, enabled to increase the IPCE value up to 70% at 430 nm. If the IPCE value of photoanode is assumed as 100%, the maximum theoretical photocurrents of the photoanodes (J_{abs}) could be calculated based on the data of solar spectral (ASTMG173–03) [30,31]. For pristine $BiVO_4$, CFCOS/$BiVO_4$, COFs/$BiVO_4$ and heterostructured CFCOS/COFs/$BiVO_4$ photoanodes, their theoretical J_{abs} were estimated to be 7.2, 10.7, 10.1 and 11.5 mA cm^{-2}, respectively (Fig. 5c and Text S4). Therefore, combing with the actual IPCE values, the calculated photocurrent densities of $BiVO_4$, CFCOS/$BiVO_4$, COFs/$BiVO_4$ and CFCOS/COFs/$BiVO_4$ photoanodes were 1.6, 4.2, 3.8 and 5.4 mA cm^{-2}, respectively (Fig. 5b, d). This result is well close to the actually measured photocurrent densities (Fig. 4a), manifesting the reliability of our test data.

3.3. Kinetics of charge transfer

As well known, the PEC performance of photoanode is restricted by photoabsorption ability, charge separation efficiency and charge injection efficiency at the electrode/electrolyte interface [32,33]. The light absorption ability of samples was first investigated by UV–vis DRS spectra. Obviously, the successive modification of COFs and CFCOS onto $BiVO_4$ surface induced its absorption edge to shift from 500 nm to 550 nm and the bandgap to be narrowed from 2.47 eV ($BiVO_4$) to 2.31 eV (CFCOS/COFs/$BiVO_4$) (Figs. 6a and S7) [34]. To further demonstrate the essentially improved photo absorption efficiency of heterostructured CFCOS/COFs/$BiVO_4$ photoanode, the light harvesting efficiency was also calculated from Text S4. In contrast to pristine $BiVO_4$, CFCOS/COFs/$BiVO_4$ exhibited the optimal light harvesting efficiency (Fig. 6b), suggesting that the introduction of CFCOS and COFs did improve the light absorption efficiency of pristine $BiVO_4$. The charge injection and separation efficiency of the modified $BiVO_4$ was further investigated [35,36]. The detailed calculation of charge injection and charge separation efficiency are given in the Supporting Information (Text S4). The loading of CFCOS co-catalyst on $BiVO_4$ surface prominently increased the charge injection efficiency from 34.28% to 54.26% at 1.23 V vs. RHE (Fig. 6c). Based on the results of Figs. 4b and 5c, the charge separation efficiency curves of all samples show no significant difference in Fig. 6d, which was ascribed to the increased theoretical photocurrent and the inherent charge accumulation at different interfaces [37], implying the active role of COFs interlayer in promoting effective charge separation at the interface between CFCOS and $BiVO_4$, consistent with the results of I-t curves. Luckily, the construction of heterostructured CFCOS/COFs/$BiVO_4$ photoanode with COFs as an interlayer could overcome these negative limitations by boosting the charges′ separation and improving the charge injection efficiency up to 69.8% at 1.23 V vs. RHE, respectively. All these results clearly

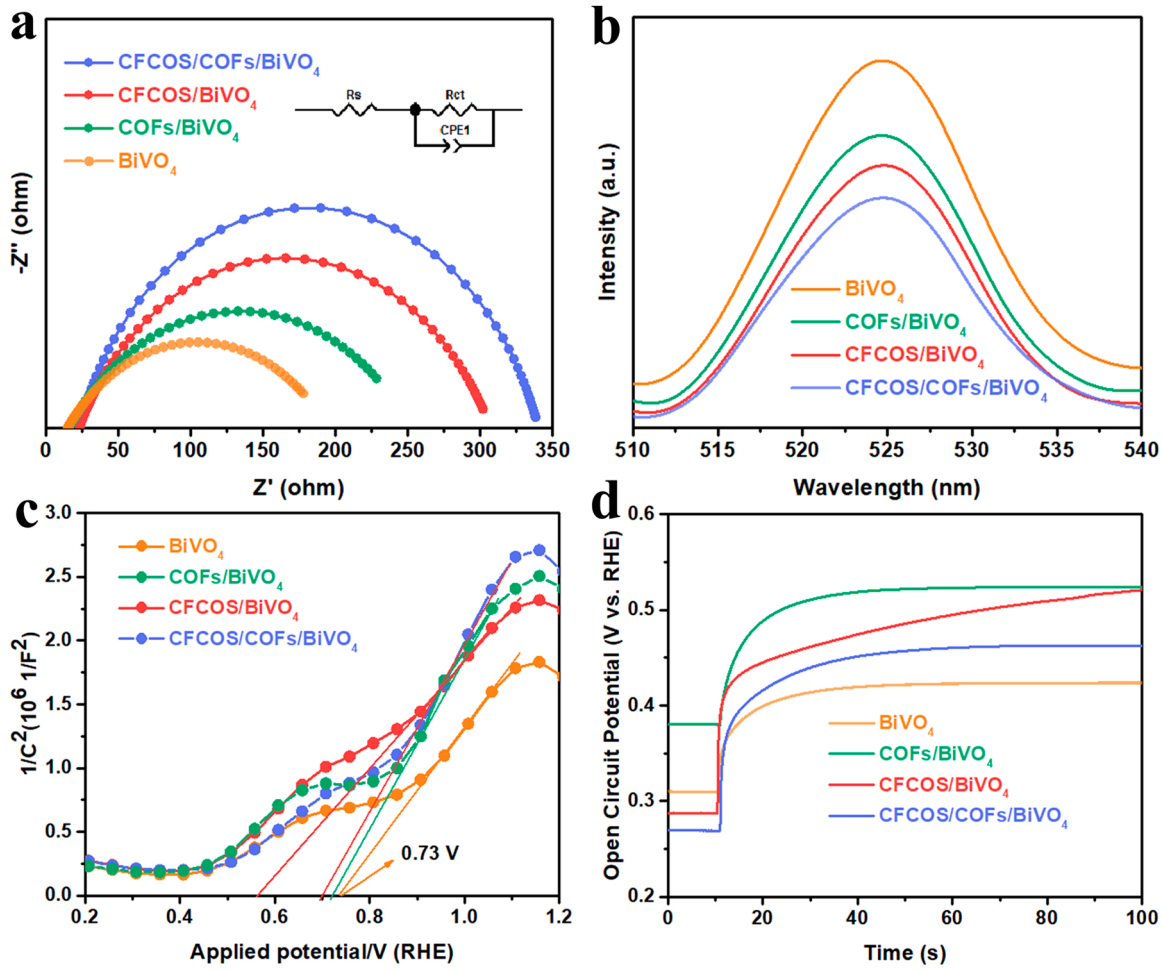

Fig. 7. (a) EIS at 1.23 V vs. RHE, (b) PL spectra, (c) Mott-Schottky plots at room temperature in dark and (d) Open-circuit potentials (Voc) versus time curves of $BiVO_4$, $COFs/BiVO_4$, $CFCOS/BiVO_4$ and $CFCOS/COFs/BiVO_4$ electrodes in dark.

demonstrated that heterostructured $CFCOS/COFs/BiVO_4$ photoanode with CFCOS co-catalyst and COFs interlayer might simultaneously extend light absorption ability, accelerate charge separation and enhance charge injection, finally contributing to PEC water oxidation.

To experimentally support these results, the charge kinetics of heterostructured $CFCOS/COFs/BiVO_4$ photoanode was investigated by electrochemical impedance spectrum (EIS) at 1.23 V vs. RHE. The EIS plots in Fig. 7a were fitted based on the equivalent circuit model, where Rs represents the electrolyte resistance, CPE is the constant phase angle element, and Rct is the interfacial charge transfer resistance between semiconductors and electrolytes [38]. Compared with pristine $BiVO_4$, $CFCOS/BiVO_4$ and $COFs/BiVO_4$ photoanodes, heterostructured CFCOS/COFs/$BiVO_4$ photoanode showed the smallest R_{ct} (Table S3), manifesting its excellent charge transfer kinetic. The boosted charge separation efficiency was further checked by the steady-state photoluminescence (PL) spectra under ambient conditions. The significantly decreased maximum PL intensity of heterostructured CFCOS/COFs/$BiVO_4$ photoanode demonstrated that the severe electron-hole pairs′ recombination of pristine $BiVO_4$ was effectively suppressed (Fig. 7b) [39]. The effect of dual loading of COFs and CFCOS onto $BiVO_4$ surface was further analyzed by testing the Mott-Schottky curves in dark. The positive slopes indicated that all samples are the n-type semiconductors (Fig. 7c). By extrapolating the linear part of Mott-Schottky curves, the flat-band potential (V_{FB}) of $BiVO_4$ photoanode was estimated as 0.10 V vs. RHE. According to the relation between RHE and NHE ($E_{RHE} = E_{NHE} + 0.059$ pH), the E_{CB} of $BiVO_4$ photoanode was calculated to be 0.17 V vs. NHE. After co-modified with CFCOS and COFs, the V_{FB} of $BiVO_4$ photoanode shifted to more negative position, thus boosting electrons′ migration from CFCOS to $BiVO_4$. According to the calculated carrier concentrations, heterostructured CFCOS/COFs/$BiVO_4$ film exhibited the highest charge carrier density (Table S4), in accordance with its superior carrier interface injection efficiency. Moreover, the thermodynamic surface carrier charge transfer process of photoanodes was investigated by the open circuit potential (OCP)decay profiles tests. The positive potential of OCP decay profile indicated the upward energy band bending near the solid/liquid interface (Fig. 7d). Based on the definition of photovoltage (ΔOCP ($OCP_{dark} - OCP_{light}$)), the amount of energy band bending under light irradiation and in dark was also calculated [40]. The larger ΔOCP of heterostructured $CFCOS/COFs/BiVO_4$ photoanode firmly affirmed its accelerated surface charge carriers transfer ability (Fig. S8) [41,42].

To evaluate the practical application potential of heterostructured $CFCOS/COFs/BiVO_4$ photoanode for PEC water splitting. The actual H_2 and O_2 production amounts of these samples were monitored by gas chromatography at 1.23 V vs. RHE. It is noteworthy that the H_2 and O_2 production were positively related to the reaction time (Fig. 8a-b). The accumulated H_2 and O_2 amounts of heterostructured CFCOS/COFs/$BiVO_4$ photoanode within 3 h reached at 234.30 μmol cm^{-2} and 117.15 μmol cm^{-2} (Fig. 8c), respectively, which are 19 times higher than pristine $BiVO_4$. During the long-term PEC water splitting test, the photocurrent of pristine $BiVO_4$ photoanode without any materials deposition rapidly decayed and the final photocurrent density was less than 10% of the initial. In contrast, the co-modification of CFCOS and COFs onto $BiVO_4$ surface suppressed the decreasing of photocurrent and

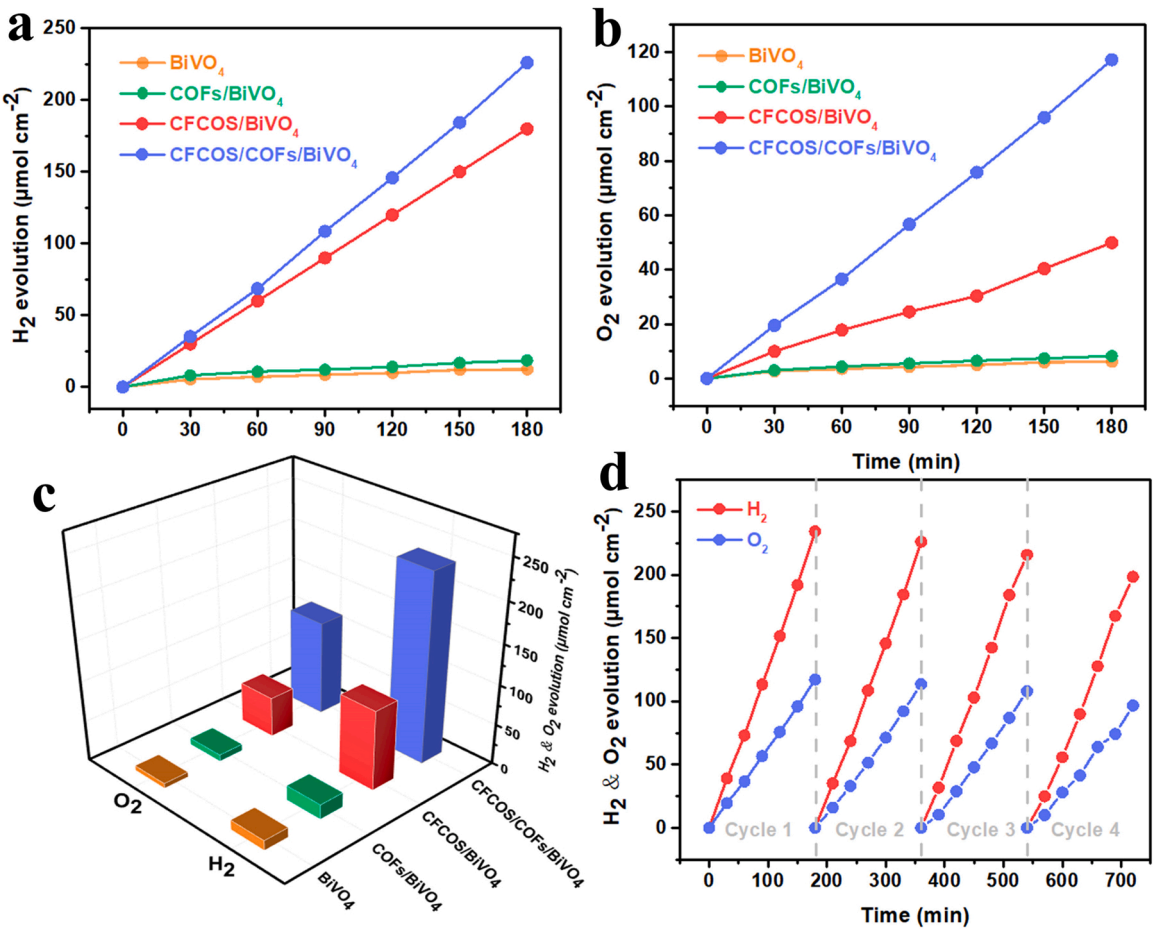

Fig. 8. (a,b) Time-resolved H_2 and O_2 production, (c) comparison of H_2 and O_2 evolution over $BiVO_4$, $COFs/BiVO_4$, $CFCOS/BiVO_4$ and $CFCOS/COFs/BiVO_4$ electrodes. (d) Long-term PEC H_2 and O_2 production of $CFCOS/COFs/BiVO_4$ photoanode.

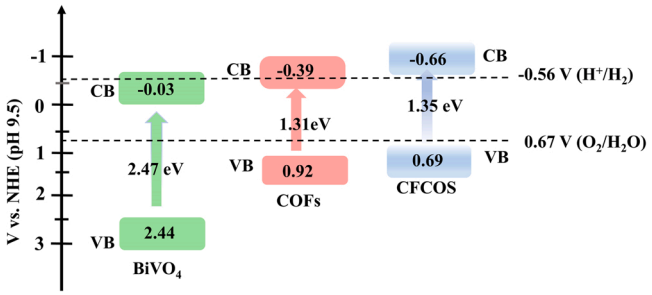

Fig. 9. The band structure of $CFCOS/COFs/BiVO_4$ photoanode.

achieved a superior PEC water splitting performance (Figs. 8d and S9). Compared with the XRD pattern of fresh $CFCOS/COFs/BiVO_4$ photoanode, no obvious change could be observed from the used sample (Fig. S10). Moreover, the used $CFCOS/COFs/BiVO_4$ photoanode almost maintained the pristine morphology (Fig. S11). All these results manifested the outstanding photostability of heterostructured $CFCOS/COFs/BiVO_4$ photoanode.

3.4. Mechanism analysis

To analyze the promotion mechanism of heterostructured $CoFe_{1.5}Cr_{0.5}S_3O/COFs/BiVO_4$ photoanode for PEC water splitting, the energy band structures of CFCOS and COFs were determined (Fig. S12–13). The band gaps of CFCOS and COFs were about 1.35 and 1.31 eV, respectively. While the V_{FB} of CFCOS and COFs photoanodes were estimated to be 0.37 V and 1.05 V vs. RHE. Given that the E_{VB} of p-type semiconductors and the E_{CB} of n-type semiconductor are close to the V_{FB} [43–45], the E_{VB} of the CFCOS and the E_{CB} of the COFs photoanode could be identified as 0.69 V vs. NHE and − 0.39 V vs. NHE. Therefore, the CB of CFCOS was calculated as − 0.66 V vs. NHE and the VB of COFs photoanode was calculated as 0.92 V vs. NHE. Consequently, the band structure of $CFCOS/COFs/BiVO_4$ photoanode is shown schematically in Fig. 9.

According to these results, a possible mechanism of heterostructured $CFCOS/COFs/BiVO_4$ photoanode for PEC water splitting was thus proposed (Fig. 10). As an intermediate layer of heterostructured photoanodes, the embedded COFs could strengthen the interfacial contact between co-catalysts and catalysts, extend the solar absorption of photoanodes to visible light region and facilitate charge carriers' transportation. Driven by the matched energy band of $CFCOS/COFs/BiVO_4$, the excited photoelectrons in the CB of CFCOS could be rapidly transferred through COFs and then enriched in $BiVO_4$, which was further transferred to Pt electrode via the external circuit to produce H_2. While the holes in the VB of $BiVO_4$ was finally transferred to CFCOS for the oxidation reaction to evolve O_2. Benefiting from the efficient electron-hole pairs' separation and boosted charge extraction, heterostructured $CFCOS/COFs/BiVO_4$ photoanode exhibited a superior PEC performance for stoichiometric H_2 and O_2 evolution, higher than the previously reported $BiVO_4$-based composite photoanodes (Table S5).

4. Conclusion

In conclusion, we demonstrated a feasible strategy to facilitate interfacial charge separation between $BiVO_4$ photoanode and CFCOS co-

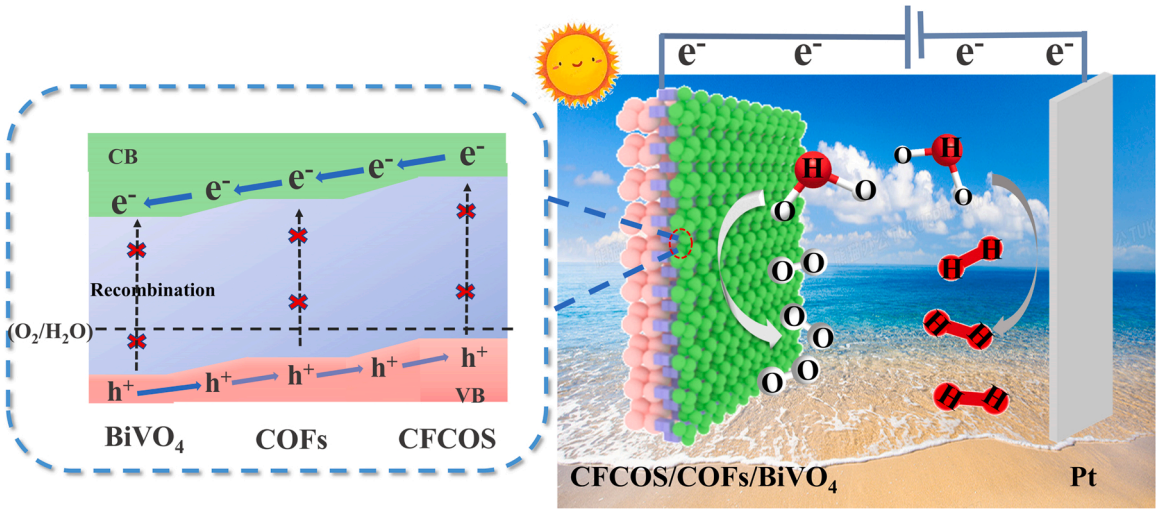

Fig. 10. Schematic mechanism of CFCOS/COFs/$BiVO_4$ photoanode for PEC water splitting.

catalyst by introducing a COFs interlayer. Compared to pristine $BiVO_4$, binary CFCOS/$BiVO_4$ and COFs/$BiVO_4$, heterostructured CFCOS/COFs/$BiVO_4$ photoanode exhibited a highest photocurrent density of 5.1 mA cm^{-2} at 1.23 V vs. RHE and a charge injection efficiency of 69.8%. Under AM 1.5 G irradiation, heterostructured CFCOS/COFs/$BiVO_4$ photoanode reached at a superior PEC water splitting efficiency with a cumulated H_2 and O_2 yields of 234.30 μmol cm^{-2} and 117.15 μmol cm^{-2} within 3 h, respectively. Through a more in-depth analysis, the improved PEC performance of heterostructured CFCOS/COFs/$BiVO_4$ photoanode was attributed to the synergistic effect between CFCOS, COFs and $BiVO_4$. That is, the successive deposition of CFCOS and COFs onto $BiVO_4$ surface can effectively broaden solar response range and enhance the absorption ability. The loaded CFCOS co-catalyst can largely lower the overpotential of water oxidation from 0.40 to 0.26 V vs. RHE. While the introduced COFs layer severed as an efficient charge transport channel to boost charge extraction from $BiVO_4$ to CFCOS. This work provides a feasible method to simultaneously optimize surface kinetics and enhance charge carrier utilization efficiency of $BiVO_4$ photoanode for efficient PEC water splitting.

Declaration of Competing Interest

The authors declare that they have no known competing financial interests or personal relationships that could have appeared to influence the work reported in this paper.

Data availability

Data will be made available on request.

Acknowledgements

This work was financially supported by the National Natural Science Foundation of China (52173277); the Innovative Research Team for Science and Technology of Shaanxi Province, China (2022TD-04); the Fundamental Research Funds for the Central Universities of Chang'an University, China (300102299304); and the Natural Science Basic Research Fund of Shaanxi Province, China (2020JZ-20).

Appendix A. Supporting information

Supplementary data associated with this article can be found in the online version at doi:10.1016/j.apcatb.2023.122921.

References

[1] H. Chai, S. Wang, X. Wang, J. Ma, J. Jin, Modulation of the chemical microenvironment at the hematite-based photoanode interface with a covalent triazine framework for efficient photoelectrochemical water oxidation, ACS Catal. 12 (2022) 3700–3709.
[2] Y. Shi, J. Li, C. Mao, S. Liu, X. Wang, X. Liu, S. Zhao, X. Liu, Y. Huang, L. Zhang, Van der waals gap-rich BiOCl atomic layers realizing efficient, pure-water CO_2-to-CO photocatalysis, Nat. Commun. 12 (2021) 5923.
[3] Y. Li, Q. Wang, X. Hu, Y. Meng, H. She, L. Wang, J. Huang, G. Zhu, Constructing NiFe-metal-organic frameworks from NiFe-layered double hydroxide as a highly efficient cocatalyst for $BiVO_4$ photoanode PEC water splitting, Chem. Eng. J. 433 (2022), 133592.
[4] L. Liu, Y. Bai, Z. Huang, G. Wang, J. Cui, H. Bai, W. Fan, Understanding the role of Ce sites for boosting PEC-NIRR without externally applied potentials, Inorg. Chem. Front. 10 (2023) 2060–2066.
[5] T. Palaniselvam, L. Shi, G. Mettela, D.H. Anjum, R. Li, K.P. Katuri, P.E. Saikaly, P. Wang, Vastly enhanced $BiVO_4$ photocatalytic OER performance by $NiCoO_2$ as cocatalyst, Adv. Mater. Interfaces 4 (2017) 1700540.
[6] J. Sun, H. Xue, Y. Zhang, X.L. Zhang, N. Guo, T. Song, H. Dong, Y. Kong, J. Zhang, Q. Wang, Unraveling the synergistic effect of heteroatomic substitution and vacancy engineering in $CoFe_2O_4$ for superior electrocatalysis performance, Nano Lett. 22 (2022) 3503–3511.
[7] B. Zhang, S. Yu, Y. Dai, X. Huang, L. Chou, G. Lu, G. Dong, Y. Bi, Nitrogen-incorporation activates NiFeOx catalysts for efficiently boosting oxygen evolution activity and stability of $BiVO_4$ photoanodes, Nat. Commun. 12 (2021) 6969.
[8] T. Soltani, A. Tayyebi, B.-K. Lee, $BiFeO_3$/$BiVO_4$ p-n heterojunction for efficient and stable photocatalytic and photoelectrochemical water splitting under visible-light irradiation, Catal. Today 340 (2020) 188–196.
[9] S.A. Monny, L. Zhang, Z. Wang, B. Luo, M. Konarova, A. Du, L. Wang, Fabricating highly efficient heterostructured $CuBi_2O_4$ photocathodes for unbiased water splitting, J. Mater. Chem. A 8 (2020) 2498–2504.
[10] Y. Li, Q. Mei, Z. Liu, X. Hu, Z. Zhou, J. Huang, B. Bai, H. Liu, F. Ding, Q. Wang, Fluorine-doped iron oxyhydroxide cocatalyst: promotion on the WO_3 photoanode conducted photoelectrochemical water splitting, Appl. Catal. B 304 (2022), 120995.
[11] L. Wang, H. Cheng, Z. Zhang, Y. Zhang, J. Huang, H. She, L. Liu, Q. Wang, Rational design of honeycomb-like APTES-TiO_2/COF heterostructures: Promoted intramolecular charge transfer for visible-light-driven catalytic CO_2 reduction, Chem. Eng. J. 456 (2023), 140990.
[12] J. Huang, Y. Wang, K. Chen, T. Liu, Q. Wang, Boosting the photoelectrochemical water oxidation performance of bismuth vanadate by $ZnCo_2O_4$ nanoparticles, Chin. Chem. Lett. 33 (2022) 2060–2064.
[13] C. Feng, Q. Zhou, B. Zheng, X. Cheng, Y. Zhang, Y. Bi, Ultrathin $NiCo_2O_4$ nanosheets with dual-metal active sites for enhanced solar water splitting of a $BiVO_4$, Photo, J. Mater. Chem. A 7 (2019) 22274–22278.
[14] J. Ma, H. Chi, A. Wang, P. Wang, H. Jing, T. Yao, C. Li, Identifying and removing the interfacial states in metal-oxide-semiconductor schottky Si photoanodes for the highest fill factor, J. Am. Chem. Soc. 144 (2022) 17540–17548.
[15] L. Wang, R. Lian, Y. Zhang, X. Ma, J. Huang, H. She, C. Liu, Q. Wang, Rational preparation of cocoon-like g-C_3N_4/COF hybrids: Accelerated intramolecular charge delivery for photocatalytic hydrogen evolution, Appl. Catal. B 315 (2022), 121568.
[16] S. Chatterjee, P. Bhanja, D. Ghosh, P. Kumar, S. Kanti Das, S. Dalapati, A. Bhaumik, Metformin-templated nanoporous ZnO and covalent organic framework heterojunction photoanode for photoelectrochemical water oxidation, ChemSusChem 14 (2021) 408–416.

[17] H. Sun, W. Hua, Y. Li, J.-G. Wang, Conformal coating of superhydrophilic metal-organic complex toward substantially improved photoelectrochemical water oxidation, Chem. Eng. J. 427 (2022), 131004.
[18] S.R. Peurifoy, J.C. Russell, T.J. Sisto, Y. Yang, X. Roy, C. Nuckolls, Designing three-dimensional architectures for high-performance electron accepting pseudocapacitors, J. Am. Chem. Soc. 140 (2018) 10960–10964.
[19] S. Bhunia, S.K. Das, R. Jana, S.C. Peter, S. Bhattacharya, M. Addicoat, A. Bhaumik, A. Pradhan, Electrochemical stimuli-driven facile metal-free hydrogen evolution from pyrene-porphyrin-based crystalline covalent organic framework, ACS Appl. Mater. Interfaces 9 (2017) 23843–23851.
[20] X. Fan, F. Kong, A. Kong, A. Chen, Z. Zhou, Y. Shan, Covalent porphyrin framework-derived Fe_2P@Fe_4N-coupled nanoparticles embedded in N-doped carbons as efficient trifunctional electrocatalysts, ACS Appl. Mater. Interfaces 9 (2017) 32840–32850.
[21] Y. Yan, T. He, B. Zhao, K. Qi, H. Liu, B.Y. Xia, Metal/covalent-organic frameworks-based electrocatalysts for water splitting, J. Mater. Chem. A 6 (2018) 15905–15926.
[22] M. Wang, Z. Wang, B. Zhang, W. Jiang, X. Bao, H. Cheng, Z. Zheng, P. Wang, Y. Liu, M.-H. Whangbo, Y. Li, Y. Dai, B. Huang, Enhancing the photoelectrochemical water oxidation reaction of $BiVO_4$ photoanode by employing carbon spheres as electron reservoirs, ACS Catal. 10 (2020) 13031–13039.
[23] J.B. Pan, B.H. Wang, J.B. Wang, H.Z. Ding, W. Zhou, X. Liu, J.R. Zhang, S. Shen, J. K. Guo, L. Chen, Activity and stability boosting of an oxygen-vacancy-rich $BiVO_4$ photoanode by NiFe-MOFs thin layer for water oxidation, Angew. Chem., Int. Ed. 133 (2021) 1453–1460.
[24] S. Jin, X. Ma, J. Pan, C. Zhu, S.E. Saji, J. Hu, X. Xu, L. Sun, Z. Yin, Oxygen vacancies activating surface reactivity to favor charge separation and transfer in nanoporous $BiVO_4$ photoanodes, Appl. Catal. B 81 (2021), 119477.
[25] B. Zhang, W. Wang, L. Liang, Z. Xu, X. Li, S. Qiao, Prevailing conjugated porous polymers for electrochemical energy storage and conversion: lithium-ion batteries, supercapacitors and water-splitting, Coord. Chem. Rev. 436 (2021), 213782.
[26] Y. Shi, Z. Yang, L. Shi, H. Li, X. Liu, X. Zhang, J. Cheng, C. Liang, S. Cao, F. Guo, X. Liu, Z. Ai, L. Zhang, Surface boronizing can weaken the excitonic effects of BiOBr nanosheets for efficient O_2 activation and selective NO oxidation under visible light irradiation, Environ. Sci. Technol. 56 (2022) 14478–14486.
[27] Y. Shi, G. Zhan, H. Li, X. Wang, X. Liu, L. Shi, K. Wei, C. Ling, Z. Li, H. Wang, C. Mao, X. Liu, L. Zhang, Simultaneous manipulation of bulk excitons and surface defects for ultrastable and highly selective CO_2 photoreduction, Adv. Mater. 33 (2021) 2100143.
[28] Y. Song, X. Zhang, Y. Zhang, P. Zhai, Z. Li, D. Jin, J. Cao, C. Wang, B. Zhang, J. Gao, L. Sun, J. Hou, Engineering MoOx/MXene hole transfer layers for unexpected boosting of photoelectrochemical water oxidation, Angew. Chem., Int. Ed. 61 (2022) 202200946.
[29] K. Zhang, B. Jin, C. Park, Y. Cho, X. Song, X. Shi, S. Zhang, W. Kim, H. Zeng, J. H. Park, Black phosphorene as a hole extraction layer boosting solar water splitting of oxygen evolution catalysts, Nat. Commun. 10 (2019) 2001.
[30] H. She, P. Yue, J. Huang, L. Wang, Q. Wang, One-step hydrothermal deposition of F:FeOOH onto $BiVO_4$ photoanode for enhanced water oxidation, Chem. Eng. J. 392 (2020), 123703.
[31] J. Zhang, X. Wei, J. Zhao, Y. Zhang, L. Wang, J. Huang, H. She, Q. Wang, Electronegative Cl^- modified $BiVO_4$ photoanode synergized with nickel hydroxide cocatalyst for high-performance photoelectrochemical water splitting, Chem. Eng. J. 454 (2023), 140081.
[32] Y. Zhang, H. Lv, Z. Zhang, L. Wang, X. Wu, H. Xu, Stable unbiased photo-electrochemical overall water splitting exceeding 3% efficiency via covalent triazine framework/metal oxide hybrid photoelectrodes, Adv. Mater. 33 (2021) 2008264.
[33] S. Wang, G. Liu, L. Wang, Crystal facet engineering of photoelectrodes for photoelectrochemical water splitting, Chem. Rev. 119 (2019) 5192–5247.
[34] S. Kim, T.A. Dela Pena, S. Seo, H. Choi, J. Park, J.-H. Lee, J. Woo, C.H. Choi, S. Lee, Co-catalytic effects of Bi-based metal-organic framework on $BiVO_4$ photoanodes for photoelectrochemical water oxidation, Appl. Surf. Sci. 563 (2021), 150357.
[35] J. Pan, B. Wang, J. Wang, H. Ding, W. Zhou, X. Liu, J. Zhang, S. Shen, J. Guo, L. Chen, C. Au, L. Jiang, S. Yin, Activity and stability boosting of an oxygen-vacancy-rich $BiVO_4$ photoanode by NiFe-MOFs thin layer for water oxidation, Angew. Chem., Int. Ed. 60 (2021) 1433–1440.
[36] Q. Pan, A. Li, Y. Zhang, Y. Yang, C. Cheng, 3D brochosomes-like TiO_2/WO_3/$BiVO_4$ arrays as photoanode for photoelectrochemical hydrogen production, Small 15 (2019) 1900924.
[37] Y. Wang, J. Huang, L. Wang, H. She, Q. Wang, Research progress of ferrite materials for photoelectrochemical water splitting, Chin. J. Struct. Chem. 41 (2022) 2201054–2201068.
[38] C. Xu, W. Sun, Y. Dong, C. Dong, Q. Hu, B. Ma, Y. Ding, A graphene oxide–molecular Cu porphyrin-integrated $BiVO_4$ photoanode for improved photoelectrochemical water oxidation performance, J. Mater. Chem. A 8 (2020) 4062–4072.
[39] X. Yin, Q. Liu, Y. Yang, Y. Liu, K. Wang, Y. Li, D. Li, X. Qiu, W. Li, J. Li, An efficient heterostructured photoelectrochemical cell composed of FeOOH/TiO_2/$BiVO_4$ and Cu_2O for self-driven solar water splitting, Int. J. Hydrog. Energy 44 (2019) 594–604.
[40] X. Long, C. Wang, S. Wei, T. Wang, J. Jin, J. Ma, Layered double hydroxide onto perovskite oxide-decorated ZnO nanorods for modulation of carrier transfer behavior in photoelectrochemical water oxidation, ACS Appl. Mater. Interfaces 12 (2019) 2452–2459.
[41] H. Li, Z. Wang, H. Jing, S. Yi, S. Zhang, X. Yue, Z. Zhang, H. Lu, D. Chen, Synergetic integration of passivation layer and oxygen vacancy on hematite nanoarrays for boosted photoelectrochemical water oxidation, Appl. Catal. B 284 (2021), 119760.
[42] H. Wang, Y. Xia, H. Li, X. Wang, Y. Yu, X. Jiao, D. Chen, Highly active deficient ternary sulfide photoanode for photoelectrochemical water splitting, Nat. Commun. 11 (2020) 3078.
[43] C. Li, G. Chen, J. Sun, H. Dong, Y. Wang, C. Lv, Construction of Bi_2WO_6 homojunction via QDs self-decoration and its improved separation efficiency of charge carriers and photocatalytic ability, Appl. Catal. B. 160 161 (2014) 383–389.
[44] L. Wu, M. Wang, T. Han, B. Yang, L. Geng, J. Jin, Fabrication of Fe_2O_3/$BiVO_4$ heterojunction by doping method to improve the solar water splitting performance of $BiVO_4$, J. Alloy. Compd. 949 (2023), 169822.
[45] H. Xu, D. Xu, S. Deng, D. Li, T. Jiang, L. Li, W. Fan, Y. Lei, W. Shi, Photochemical and electrochemical co-regulation of the $BiVO_4$ photoanode for water splitting, ChemComm 59 (2023) 3435–3438.